# APPENDIX B

# EXPERIMENTAL WORK

Full details on the tests that were conducted as part of this research are given in this appendix. This appendix can be seen as a separate document describing the practical tools used to assess the performance of the vehicle/track system. Not only are factors such as the influence of axle load, vehicle speed and accumulating traffic on the performance of the vehicle/track system investigated, but full details are given on the test that was designed to simultaneously measure the performance of the vehicle and the track. An important contribution to track research in particular is the measurement and interpretation of the dynamic track stiffness under a variety of circumstances.

## B.1 ROLLING STOCK

In this section the rolling stock that was used in the test train and that of the general traffic passing over the test section is described. Detail with respect to the suspension of the bogie of the test vehicle and vehicle instrumentation is also given.

### B.1.1 Test Trains and Passing Traffic

A specially configured test train was used to conduct repeatable and controlled tests as a function of deteriorating track conditions. Initially, a so-called long test train was used to evaluate the effect of axle loading on the dynamic performance of the track. This test train was made up of one Class 6E1 electric locomotive, followed by a test coach, two CCL-5 wagons loaded to 26 ton axle load, two CCL-5 wagons

loaded to 30 ton axle load, two CCL-5 wagons loaded to 20 ton axle load, and two empty CCL-5 wagons . Figure B1 shows the axle load profile of the long test train. After three days only the wagons with 26 ton axle load remained in the test train.

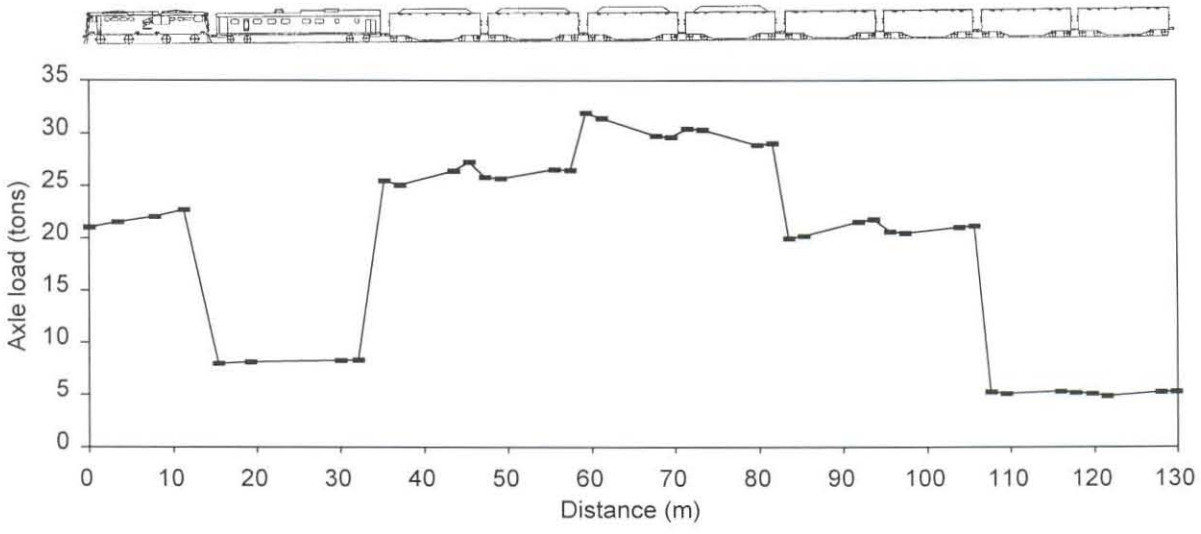


Figure B1: Loading profile of long test train.

Revenue earning traffic that passed over the test section was generally made up out of the following train configurations: 200 CCL-5 coal wagons, 100 CCL-1,2, or 3 coal wagons together with 100 CCL-5 coal wagons, or only 100 CCL-1,2, or 3 coal wagons. The loaded CCL-5 wagons have an axle load of 26 tons and the loaded CCL-1, 2 and 3 wagons have an axle load of 22 tons. These long trains were hauled by Class 7E1 or Class 11E electric locomotives with an axle load of 21 and 28 tons respectively. The distribution of the axle load over the test site after 13 MGT as obtained from traffic statistics from the Central Traffic Control Office in Vryheid is given in Figure B2. Figure B3 shows the distribution of the wheel loads as obtained from on-track measurements for two typical 200 wagon train configurations.

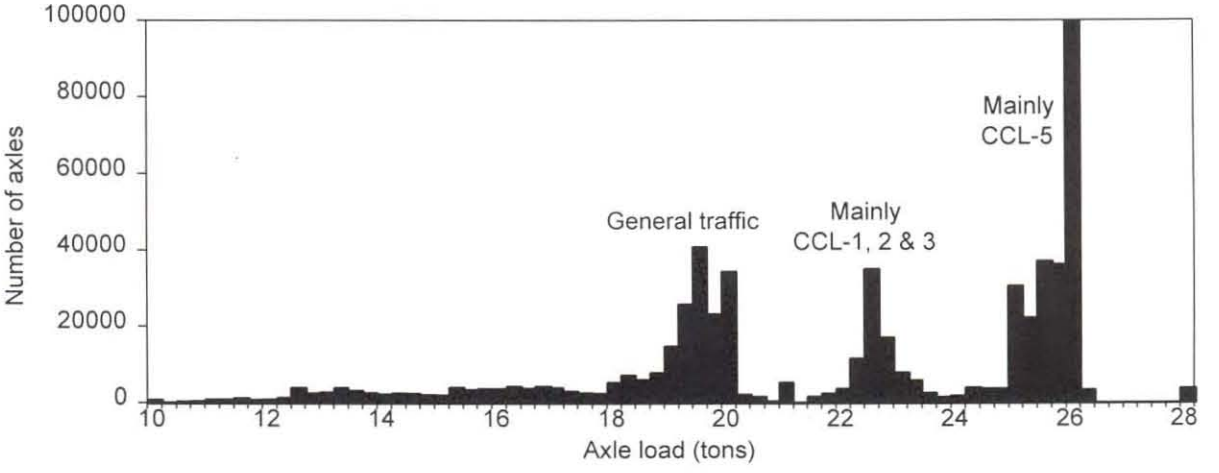


Figure B2: Axle load histogram after 13 MGT of traffic.

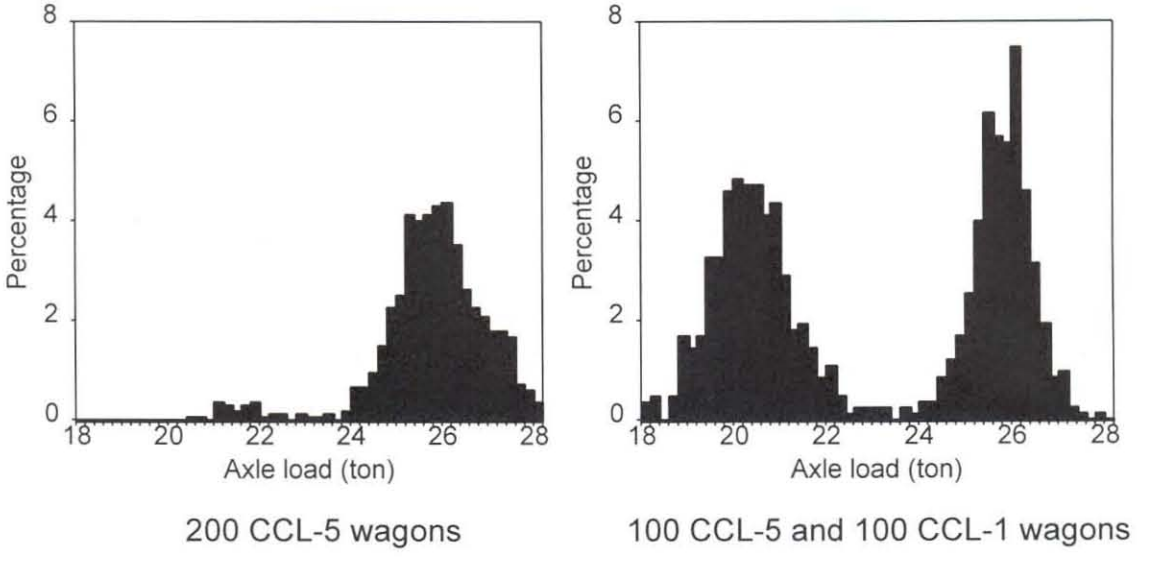


Figure B3: Axle load histograms for two typical in-service trains.

### B.1.2 CCL-5 Suspension Characteristics

The CCL-5 gondola coal wagon is equipped with two three-piece self-steering bogies of the type HS MkV which have a 26 ton axle load capacity. Pictures of the side and top view of the HS MkV bogie are given in Figure B4. In Figure B5, a drawing of the bogie is given for further clarity. From Figure B5 it can be seen that the bogie has both a primary and a secondary suspension. The primary suspension consists of two

vertically stiff (50 MN/m) rubber sandwiches per axle box. As this element is vertically very stiff, no displacement measurement were made across the element. A schematic of the secondary suspension which sits at the bolster/sideframe interface is also shown in Figure B5. The schematic clearly shows the position of the friction wedges which are resting on the stabilizer springs.

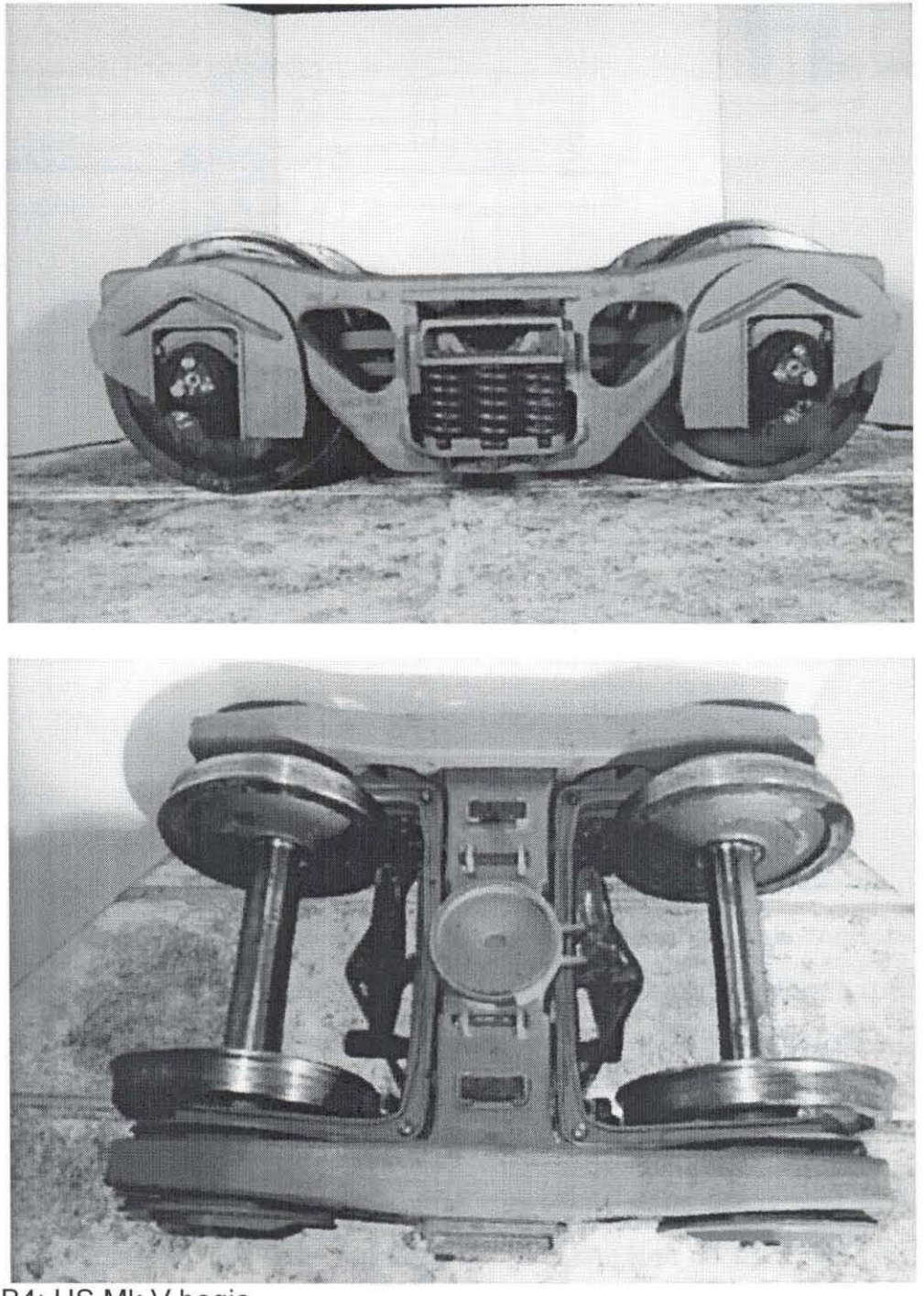

Figure B4: HS Mk V bogie.

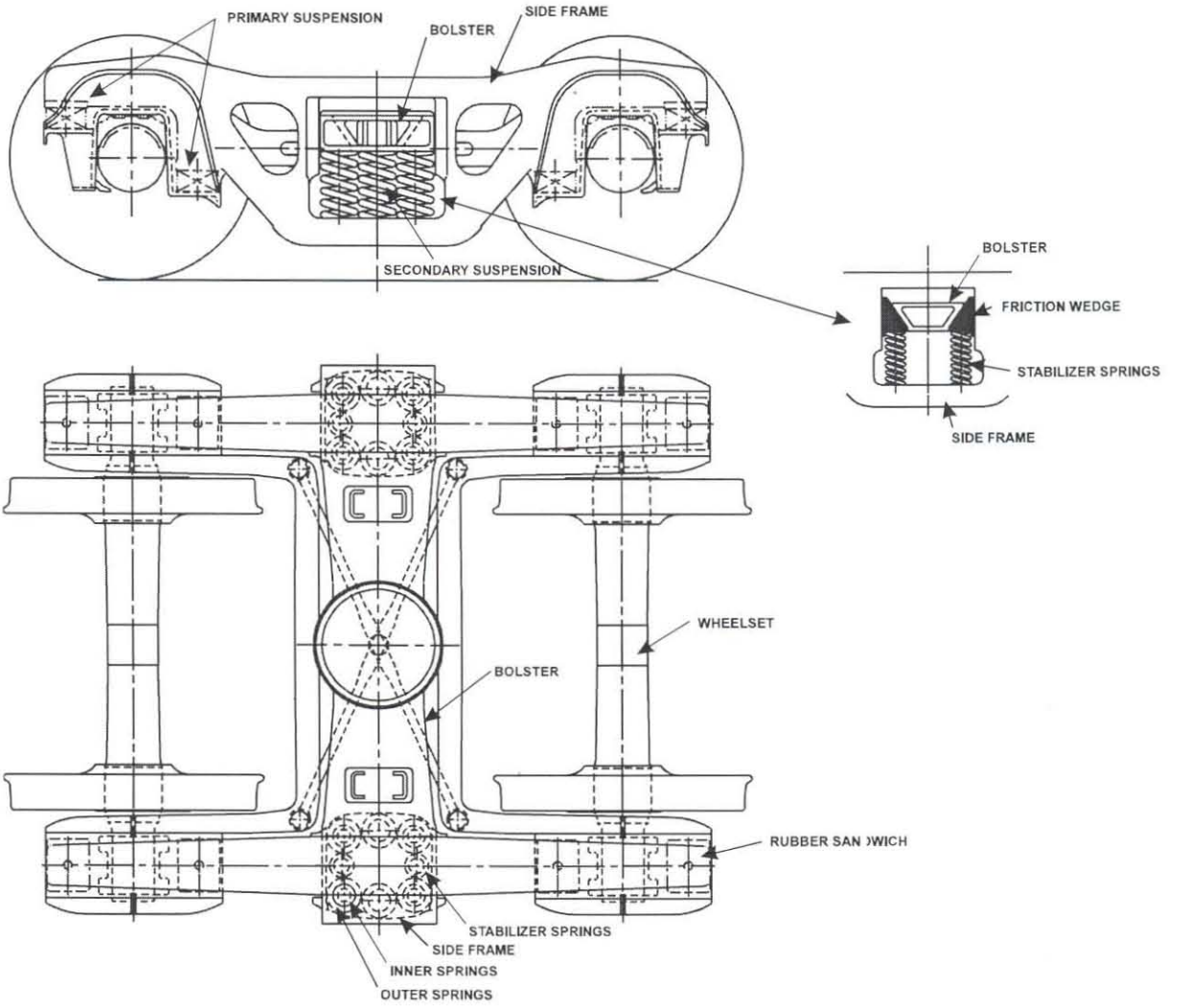


Figure B5: Drawing of a typical three-piece self-steering bogie.

The secondary suspension is designed to provide load sensitive frictional damping between the side frame and the bolster, and to keep the side frames and the bolster square relative to each other. This is achieved by the friction wedge arrangement between the bolster and the side frame pocket. The weakness of friction damping is however well recognized (Giuns, 1980; Yabuto *et al.*, 1981; Fröhling *et al.*, 1996b). The problem is that energy absorbed by friction will always be lower than the energy input for the suspension element to work. As the decay rate of frictional damping is constant, the time required for the complete decay of energy is fixed. This means that as the speed of the vehicle increases, the time of travel between

track inputs decreases but the decay of energy remains constant. Thus, when the speed exceeds a certain limit, the following energy input comes before the preceding energy input has completely decayed. Under this condition, energy input exceeds decay and there is a build-up of energy into the vehicle. When this build-up and frequency of input approaches the natural frequency of the spring-mass system, resonance occurs. A reason why the system performs as well as it does in practice, is that track causes a random rather than a harmonic input of energy.

Extensive work has been done locally and internationally on characterising the behaviour of the secondary suspension of the three-piece bogie (Urban, 1991a; Urban 1991b; Fröhling *et al.*, 1996b; Howard *et al.*, 1997). Research conducted by Spoornet has shown that load dependant friction damping can be modelled using the following definitions for the friction force, *Fff*:

$$\textit{Down stroke: If } (\dot{y}_1 - \dot{y}_2) < 0.0 \textit{ then } F_{ff} = \frac{-(x_{ss} + (y_2 - y_1))\, k_{ss}\, \mu}{\tan \alpha_w + \mu} \qquad \text{(B1)}$$

$$\textit{Up stroke: If } (\dot{y}_1 - \dot{y}_2) > 0.0 \textit{ then } F_{ff} = \frac{(x_{ss} + (y_2 - y_1))\, k_{ss}\, \mu}{\tan \alpha_w - \mu} \qquad \text{(B2)}$$

$$\textit{If } |C_{slope}(\dot{y}_1 - \dot{y}_2)| < |F_{ff}| \textit{ then } F_{ff} = C_{slope}(\dot{y}_1 - \dot{y}_2) \qquad \text{(B3)}$$

This model has been validated against test results. A comparison between the measured and the calculated hysteresis loop for a similar bogie to that used during the on-track tests is shown in Figure B6.

In an attempt to linearise the load sensitive frictional damper (Yabuto *et al.*, 1981; Fröhling *et al.*, 1996b; Howard *et al.*, 1997), it was found that this is difficult because the characteristics of any nonlinear system receiving random input is dependent on the level of energy input. The basic problem is that when the track geometry is smooth, the input from the track is small, and therefore the equivalent damping coefficient must be high. Conversely, when the track geometry is rough, the input from the track is large, and consequently the equivalent damping

coefficient must be low. In addition, vehicle speed also has an effect. The lower the vehicle speed, the greater the required equivalent damping coefficient.

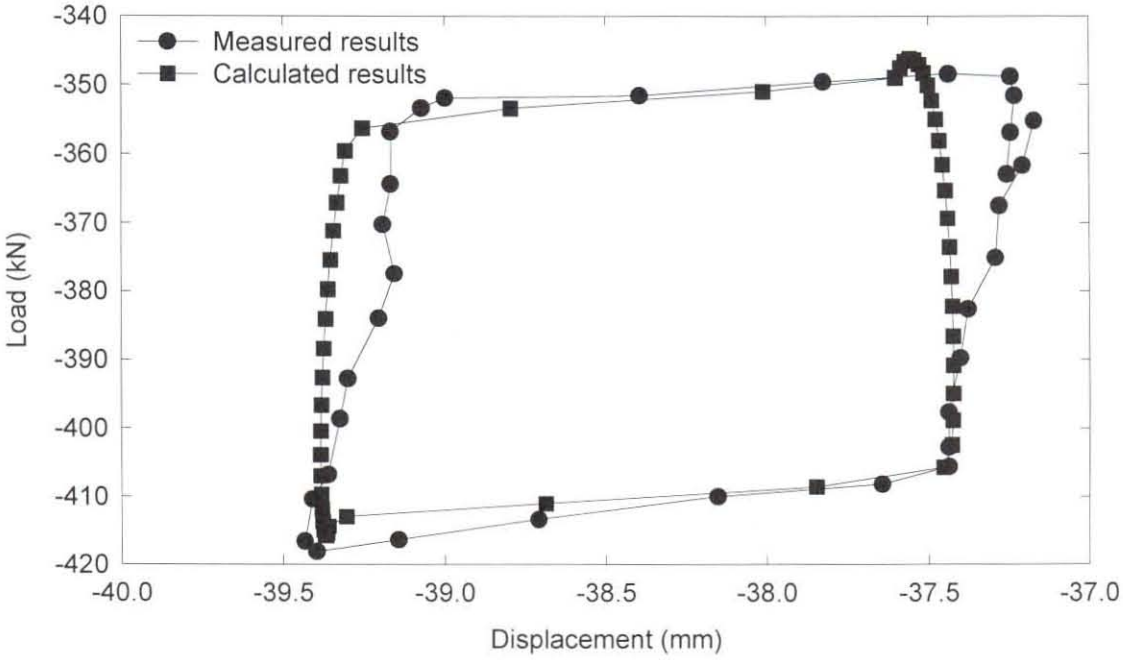


Figure B6: Measured and calculated hysteresis loop for a loaded HS Mk VII bogie.

### B.1.3 Vehicle Instrumentation

In this section the purpose of each measuring device mounted to the test vehicle is given together with a full description thereof. Samples of recorded measurements are also included together with a short interpretation of the results. The photo of the test bogie in Figure B7 shows the position of the instrumentation used during the tests.

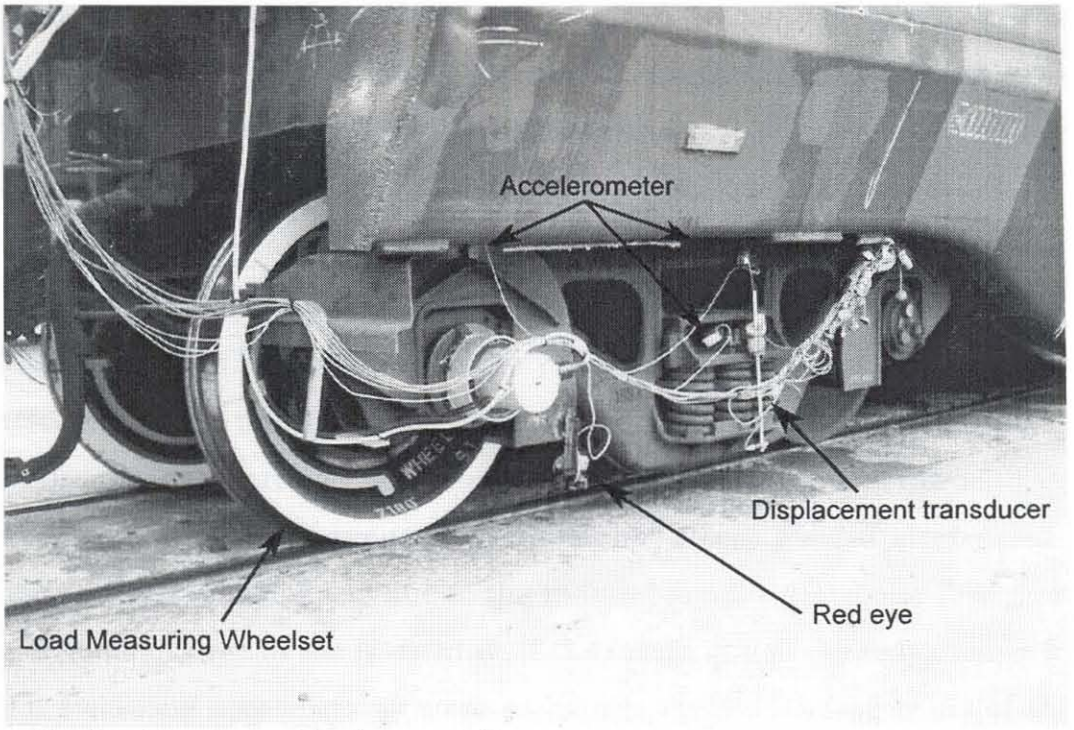


Figure B7: Test bogie and instrumentation.

*B.1.3.1 Purpose and Description*

The purpose and a brief description of the vehicle instrumentation is given below:

*Data acquisition system:* The primary elements to collect data are the instrumentation transducers, that is strain gauges, displacement transducers and accelerometers. These transducers translate the physical phenomenon of interest into an analogue signal with a calibrated relationship between the input and output quantities. This calibrated quantity is then converted into digital format and routed to a computer for real time data processing and/or storage. For the tests described in this document the CMS128 Continuous Monitoring System from TLC Software CC was used. The system is capable of sampling 128 channels at a disk spooling speed of 300kHz. During the tests, a sampling rate of 2kHz and 2.5kHz was used for the vehicle and track sensors respectively. The data was stored in a disk file which was subsequently retrieved and analysed using a post processing software module called CMSG128.

*Red eye:* The red eye was used to send out an infrared signal and pick up a reflection from reflector boards put out along the track to mark specific positions along the test track like the start and end position of the test section. The red eye was positioned 330 mm to the back of the leading wheelset of the test bogie.

*Accelerometers:* Accelerometers are electromechanical transducers which produce an electrical output proportional to the vibratory acceleration to which they are subjected. During the on-track tests, miniature Kyowa strain gauge type acceleration transducers were used to measure the vertical acceleration of various bogie components. In this type of accelerometer, strain gauges are bonded to an internal spring which deflects due to the induced accelerations and thus produces a proportional change in the resistance of the strain gauge. As indicated in Figure B7, the following accelerations were measured on the leading bogie of the test vehicle:

- Vertical acceleration of both axle boxes of the leading wheelset.
- Vertical acceleration at the centre of both side frames.
- Vertical acceleration at the left and the right outer ends of the bolster.

*Linear Variable Differential Transformer (LVDT):* LVDTs are used for measuring the displacement between two bodies. An LVDT consists of a movable magnetic core passing through a primary and two secondary coils. An Alternating Current (AC) voltage, called the excitation voltage, is applied to the primary coil, thereby inducing an AC voltage in each secondary coil, with a magnitude that depends on the proximity between the magnetic core and each secondary coil. The secondary voltages are connected in series opposition, so that the net output of the LVDT is the difference between these two voltages. When the core is at its midposition, the net output voltage is zero. When the core moves off centre, the net output voltage increases linearly in magnitude with a polarity depending on the direction of core displacement. For the tests conducted in this research two 100mm HBM LVDTs were used to measure the vertical deflection at both sides of the secondary suspension on the leading bogie.

*Load measuring wheelset:* The leading wheelset of the leading bogie was replaced by a load measuring wheelset. This wheelset was used to measure the vertical dynamic forces between the wheel and the rail. To determine the forces at the wheel/rail contact point, the load measuring wheelset is equipped with strain gauges on both the axle shaft and the wheel disk (Zeilhofer *et al.*, 1972; Ostermeyer *et al.*, 1980; Berg *et al.*, 1996). This is seen to be the correct combination for measuring the wheel/rail contact forces, because due to the variation of the wheel contact point, the lateral guiding forces as determined by the strain gauges on the axle include a systematic, analytically quantifiable error. Including the wheel disk in the measuring circuit allows an exact determination of the wheel guiding forces as well as a continuous recording of the wheel/rail contact point. Calculations are done in accordance with force and moment equilibrium equations by a digital computer.

*B.1.3.2 Sample Measurement and Interpretation*

In Figure B8, a set of measured results are given to illustrate the typical behaviour of the test vehicle over the test track. In the example given, the speed of the test vehicle was 40km/h. The two vertical lines at position B and C in the middle of the top graph indicate the position of the middle thirteen sleepers of the test site that were instrumented. The whole section between position A and D includes 150 sleepers at a 0.65 m sleeper spacing.

By comparing the vertical accelerations on the axle box with those on the side frame it can be seen that the high accelerations occurring at the axle box are significantly reduced in the side frame. This is due to primary suspension of the bogie. However, by comparing the vertical acceleration of the side frame with that of the bolster it is noticed that the acceleration of the bolster is more or less equal to the acceleration of the side frame. Hence, the secondary suspension seems to be unable to reduce the magnitude or frequency of the forces due to friction locking.

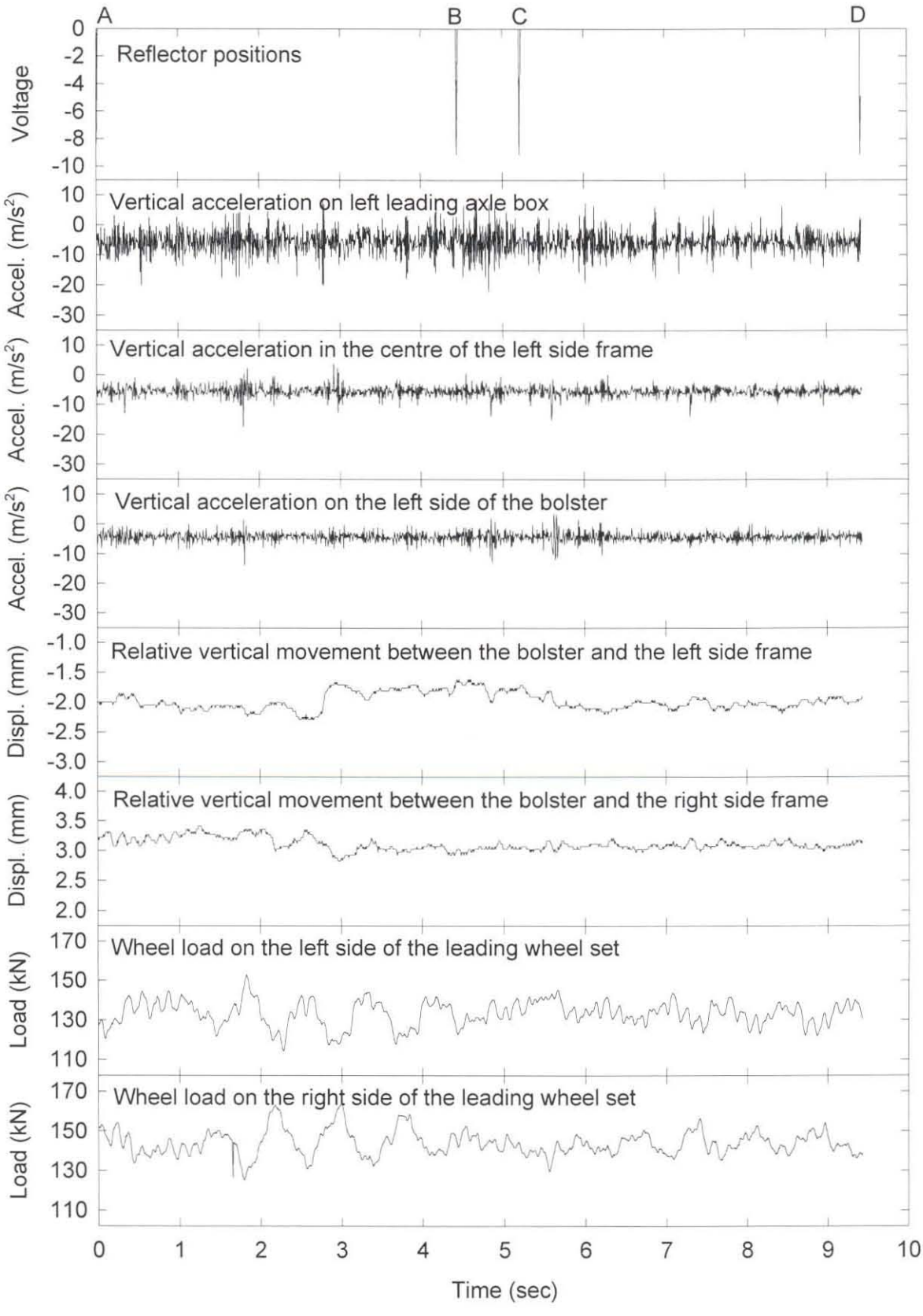


Figure B8: Measurements taken on the instrumented bogie.

Another point of interest is the fact that there is very little movement across the secondary suspension. Only about a 1mm displacement was measured in this instance. This confirms the fact that there is a high resistance to movement in the secondary suspension. A further observation can be made in terms of the measured dynamic wheel load. Here it can be seen that some rolling motion of the vehicle takes place and the dynamic wheel load component is about 20% of the static wheel load.

## B.2 INFRASTRUCTURE

In this section a description of the test site is given, followed by detail with respect to track instrumentation and measurements done.

### B.2.1 Test Site

The test site was between mast pole 7/2 and mast pole 7/4 on the line between Vryheid and Richards Bay on the Heavy Haul Coal Export Line. The test section was 150 sleepers long and the middle thirteen sleepers were instrumented to measure the dynamic behaviour of the track. Design details of the track are given in Table B1.

Table B1: Track design details.

| Parameter | Value |
|---|---|
| Sleeper length | 2200 mm |
| Sleeper spacing | 650 mm |
| Sleeper width | 259 mm |
| Sleeper area | 5.981E+004 $mm^2$ |
| Sleeper weight | 285 kg |
| Sleeper stiffness (EI) | 1.235E+004 $kN.m^2$ |
| Rail spacing | 1140 mm |
| Rail area | 7703 $mm^2$ |
| Rail weight | 60 kg/m |
| Rail stiffness (EI) | 6558 $kN.m^2$ |
| Rail fastener stiffness (HDPE rail pads) | 1.2E+006 kN/m |

The photos in Figure B9 give an overview of the track cross section at Sleeper 77 in the middle of the test section. After excavating a trench, the substructure was analysed. In Figure B10 a schematic cross section at Sleeper 77 is given. Relevant properties of the ballast samples are given in Table B2. From this information the following observations were made:

- Clean ballast was found under the sleeper while the shoulder ballast was contaminated with a substantial amount of coal.
- The bitumen layer was solid with a mixture of fowling material, ballast and bitumen.
- The bottom of the sub-ballast was 560mm and the natural soil was 770mm below the sleeper.

Site overview

Clean ballast under sleeper

Layers above and below bitumen layer

Layers down to natural soil

Figure B9: Details of the track cross section at Sleeper 77.

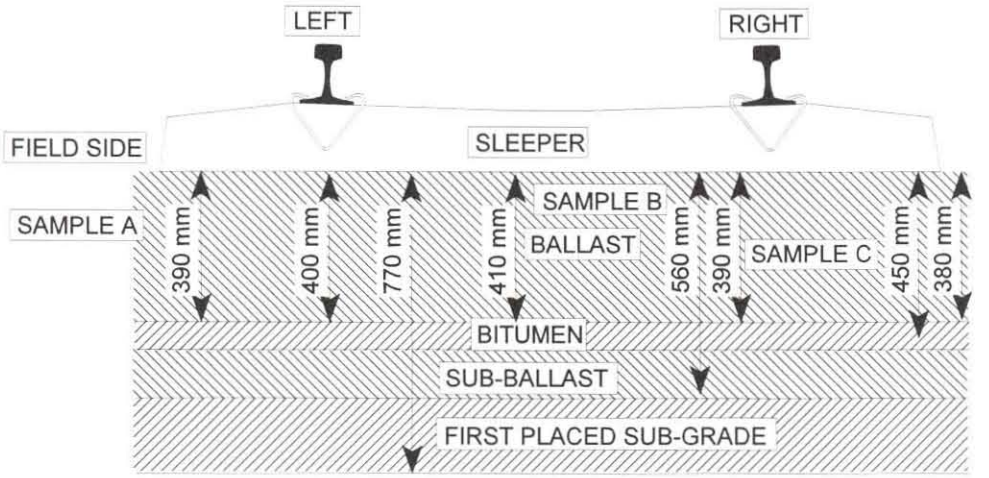


Figure B10: Schematic cross section at Sleeper 77.

Table B2: Ballast properties.

| Test | Sample A: Shoulder sample above bitumen | Sample B: Ballast under sleeper | Sample C: Ballast below sleeper under right hand rail down to bitumen layer |
|---|---|---|---|
| **L.A. Abrasion** (Specification < 22%) | 10.88% | 18.36% | 11.24% |
| **Absorption** (Specification < 1%) | 0.08% | 0.18% | 0.18% |
| **Sieve analysis** | | | |
| **Sieve size** | **% Passing** | **% Passing** | **% Passing** |
| 63.0 mm | 100.0 | 100.0 | 100.0 |
| 53.0 mm | 97.5 | 98.6 | 100.0 |
| 37.5 mm | 63.9 | 69.7 | 77.7 |
| 26.5 mm | 20.8 | 23.6 | 29.8 |
| 19.0 mm | 7.5 | 5.7 | 10.4 |
| 13.2 mm | 6.0 | 2.5 | 7.3 |
| 9.5 mm | 5.7 | 1.9 | 6.2 |
| Pan | 0.0 | 0.0 | 0.0 |

In Figure B11 the layout of the track around the selected test section is given together with the track geometry as measured with the Plasserail EMV80 track recording car. With reference to Table B3, which gives a summary of South African track standards (Permanent Way Instructions, 1984), it can be seen that the cant, the lateral alignment as well as the vertical surface profile of the track are well within the given track maintenance standard. In Figure B12 the resulting root mean square (RMS) values of the measured dynamic wheel load as calculated over 50m while the test vehicle was travelling at 70 km/h is given.

Table B3: Spoornet track standards.

| | **Construction standard A** | **Maintenance standard B** | **Safety standard C** |
|---|---|---|---|
| Vertical surface profile (7m chord) | +3mm; -3.5mm | +14mm; -14mm | +19.4mm; -19.4mm |
| Lateral alignment (10m chord) | 2.5mm | 10mm | 14mm |
| Cant | ±3mm | ±12mm | ±16mm |

In Figure B13 a selection of cross sections along the test track are shown. From the figure it is clear that the whole test section was in a cutting. The depth of the cutting increases from Sleeper 1 to Sleeper 150.

In general, track condition is defined by its functional as well as its structural condition. The functional condition is described by the geometric irregularity of the track, and the structural condition of the track is defined by the structural strength of the track components which is measured in terms of the track stiffness and the variation thereof. More information in this respect is given below.

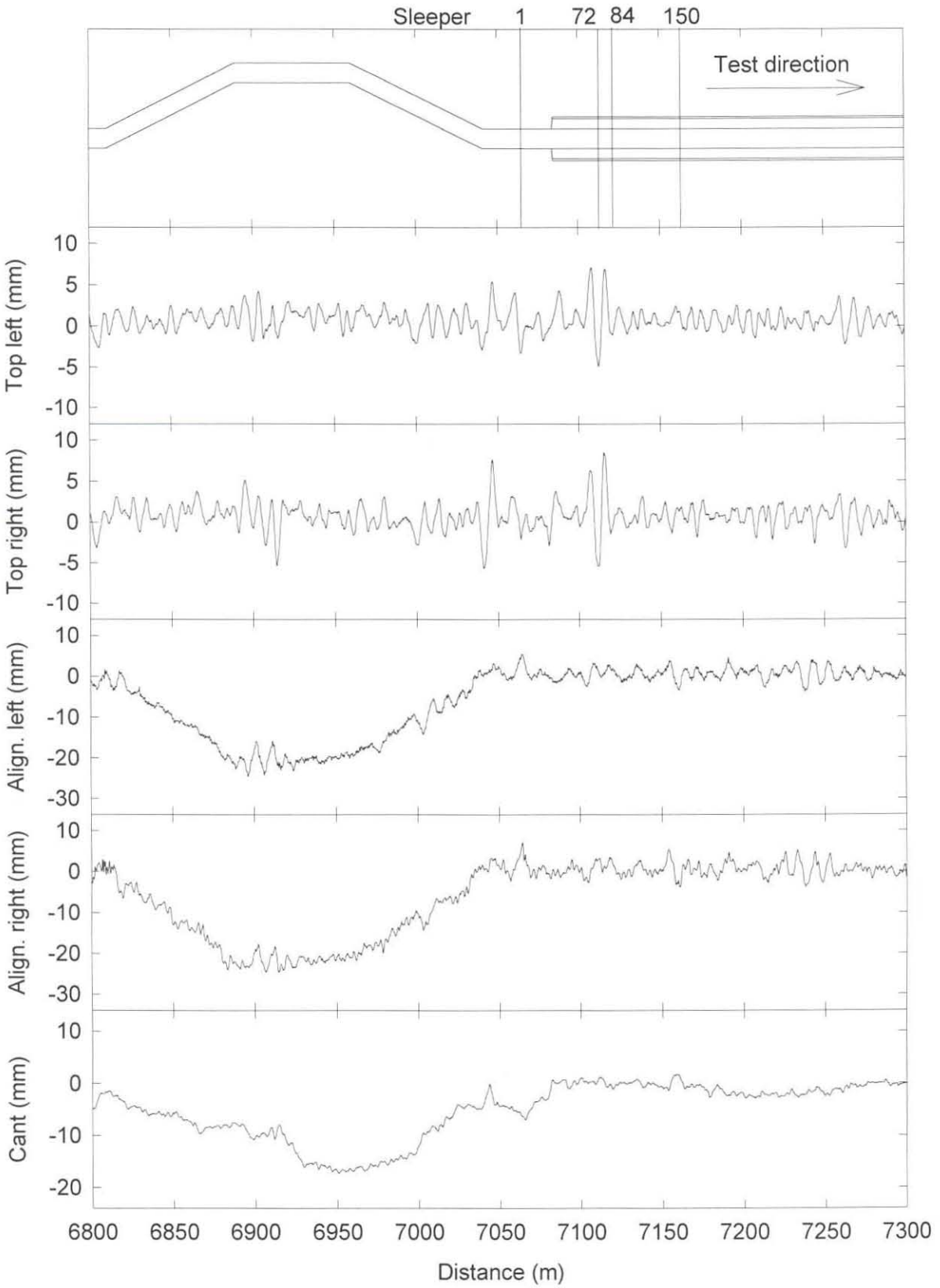


Figure B11: Track layout and geometry.

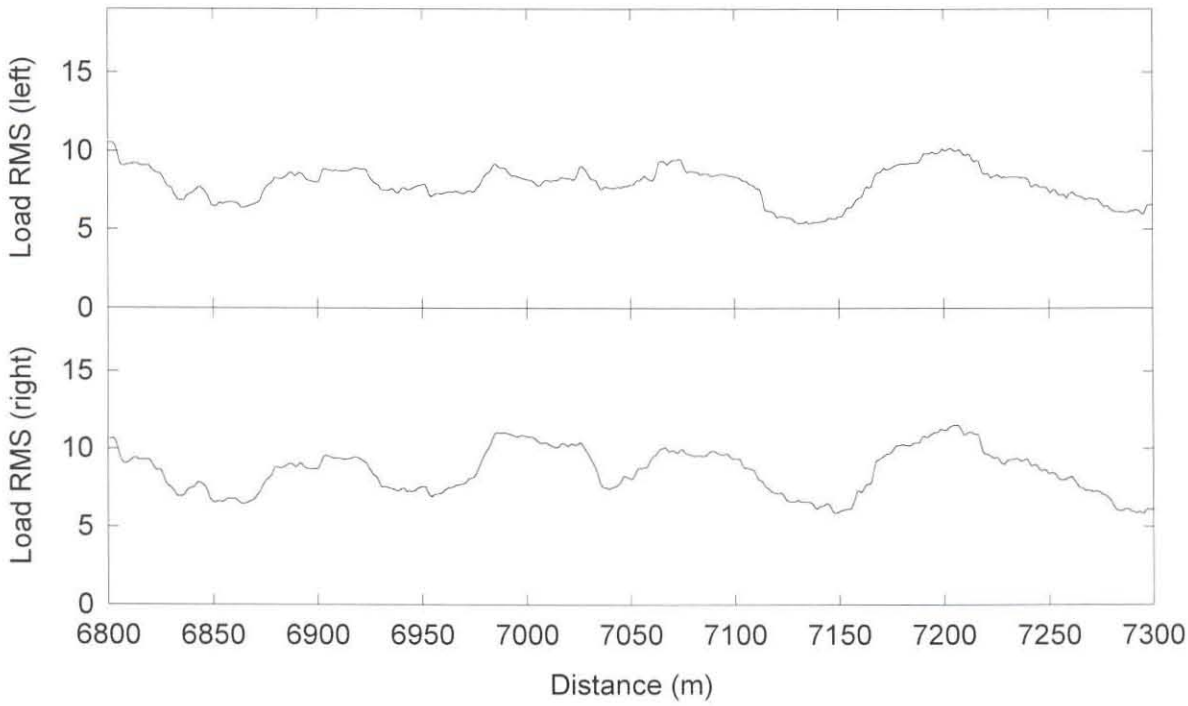


Figure B12: Root Mean Square values of the wheel load at 70km/h.

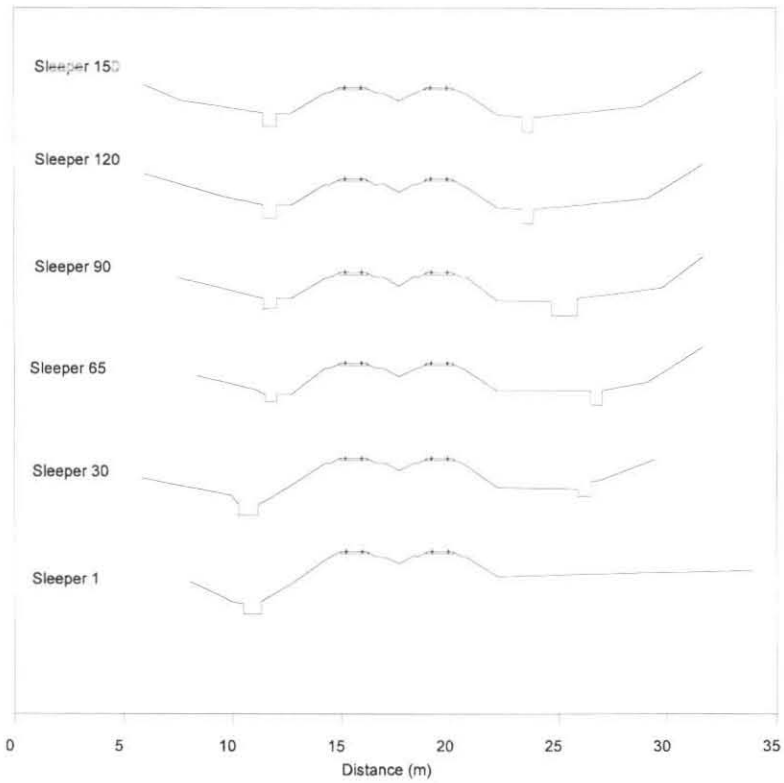


Figure B13: Cross sections at test site.

### B.2.2 Level Measurements

One of the elements describing the functional condition of the track is the vertical profile of the track. The most common methods used to measure the vertical alignment of the track are, absolute measurements, mid-chord ordinate measurements, dynamic measurement, and inertial measurements (Frederich and Hecht, 1986; Hecht, 1988). The general method used in South Africa is the mid-chord ordinate measurement method (Fröhling, 1995). Unfortunately the relationship between the fixed measuring chord length used and the variable track wavelengths causes a wavelength dependant response. Methods to obtain the "true" longitudinal track profile from such measurements have been proposed in literature (Cohen and Hutchens, 1970; Fröhling, 1995; Mauer, 1995).

For the purpose of this investigation the track geometry was only required for a short section of track and thus the absolute measuring technique was used. Measurement of the absolute unloaded vertical track profile was done with a digital level Wild NA3003 with a resolution of 0.001mm. To be able to do a settlement analysis, the track geometry measurements at each time interval were referenced to two fixed beacons on either side of the test site. Measurements were done before each test series in order to monitor the settlement of the track as a function of accumulating traffic.

### B.2.3 Static Track Stiffness Measurements

As mentioned, the structural condition of the track is primarily defined by the stiffness of the track. It is known that the stiffness of the track is generally nonlinear and varies from point to point along the track (Fröhling *et al*, 1996a). For this research the "BSSM" (Baan Styheids en Stabiliteits Meeting) track loading vehicle as shown in Figure B14 (Ebersöhn, 1995) was used. Track stiffness was measured by applying a single point load to each rail above the sleeper using two independent hydraulic cylinders (Ebersöhn and Selig, 1994) and measuring the

vertical displacement of the sleeper via a tiltmeter. The tiltmeters were mounted on a beam independent of the "BSSM" machine.

Before each measurement, the tiltmeter offset was zeroed and then simultaneous readings were taken at a zero, 29kN (3 tons), 49kN (5 tons), 78kN (8 tons) and 128kN (13 tons) load on each rail. Once the target load had been reached, a waiting period of ten seconds was required before the displacement was recorded. This was necessary to eliminate any vibrations that occurred in the beam due to the load applications by the machine. Before each test series the tiltmeters were checked with a digital level and recalibrated if required. Track stiffness measurements were conducted over the entire 150 sleeper test track and measurements were done at the same time as the track geometry measurements. Hence, a continuous measurement of the varying track support stiffness was obtained.

The unloaded vertical space curve and the loaded profile of the left and right rail as measured directly after tamping is shown in Figure B15. Figure B15 also shows the track deflection due to a 29kN and a 128kN load on the left and the right rail. From Figure B15 it can be seen that the left side is softer and has a higher stiffness variation than the right hand side. This is because the test track is on a double line and the left rail is on the field side.

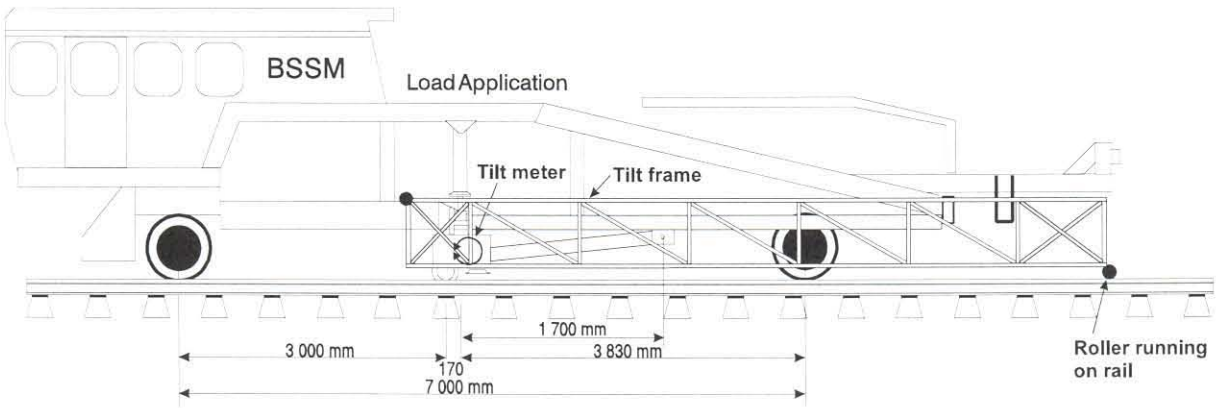


Figure B14: "BSSM" track loading vehicle.

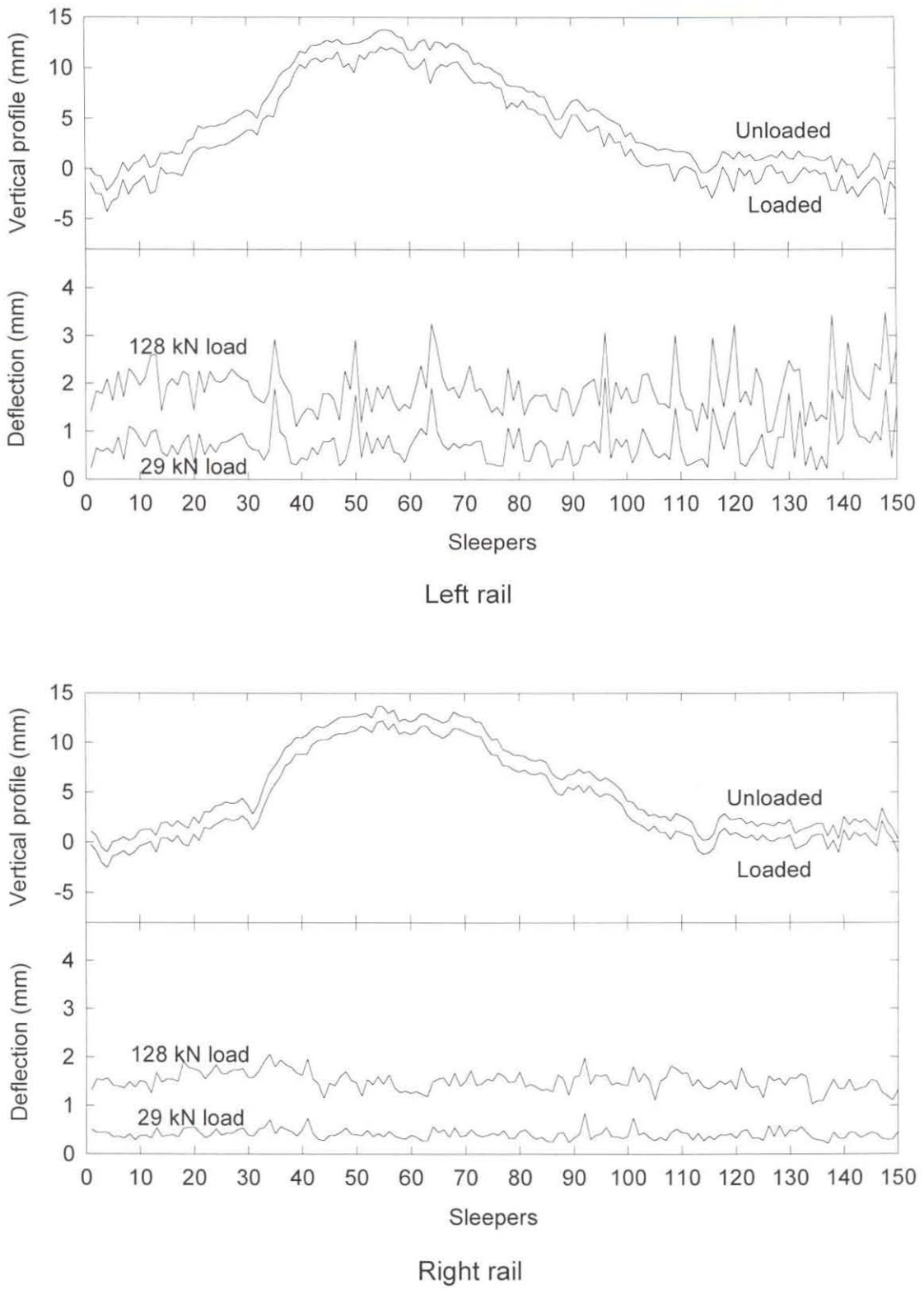


Figure B15: Unloaded and loaded vertical space curve and track deflection due to a 29kN and a 128kN load on the rail.

In Figure B16 the track deflection due to a vertical load of 29kN, 49kN, 78kN and 128kN load is shown for track with a low spatial variation in the track stiffness and track with a high variation in spatial track stiffness due to a void at Sleeper 77.

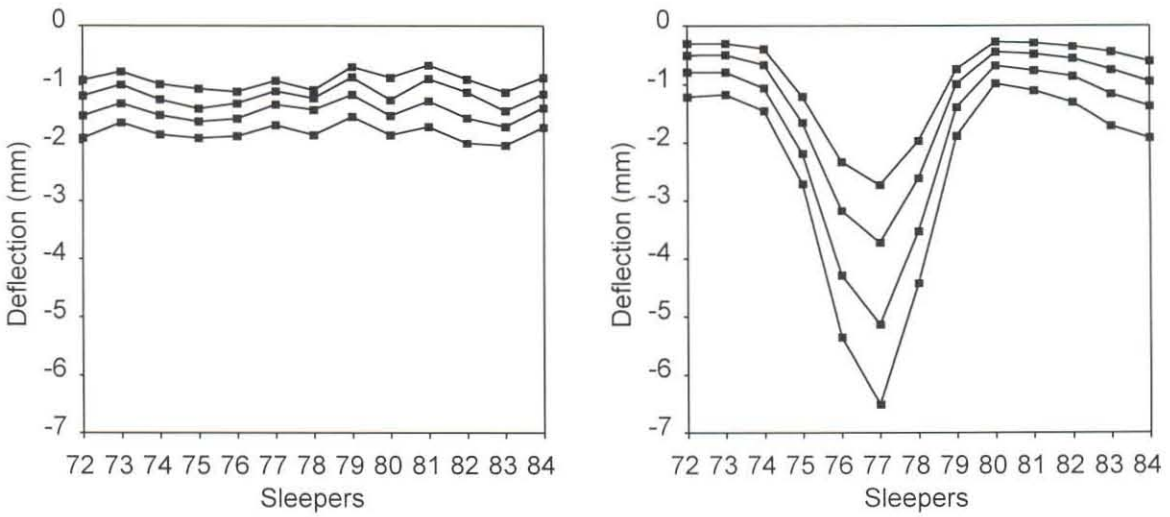


Figure B16: Track deflection due to vertical loads of 29kN, 49kN, 78kN and 128kN.

From the track stiffness measurements described in this section, a selection of static load-deflection curves are shown in Figure B17. From these curves it is clear that not only does the stiffness change from sleeper to sleeper along the track but the stiffness characteristic also changes. The initial lower slope of the nonlinear stiffness is due to voids or soft spots between the sleeper and the ballast. This initial stiffness is known as the seating stiffness. The second part of the stiffness, that is approximately between 29kN and 128kN, is called the contact stiffness and is a function of substructure stiffness properties. Here the relationship between load and deflection is found to be more linear, although in some cases stiffening is observed (Ebersöhn *et al.*, 1993).

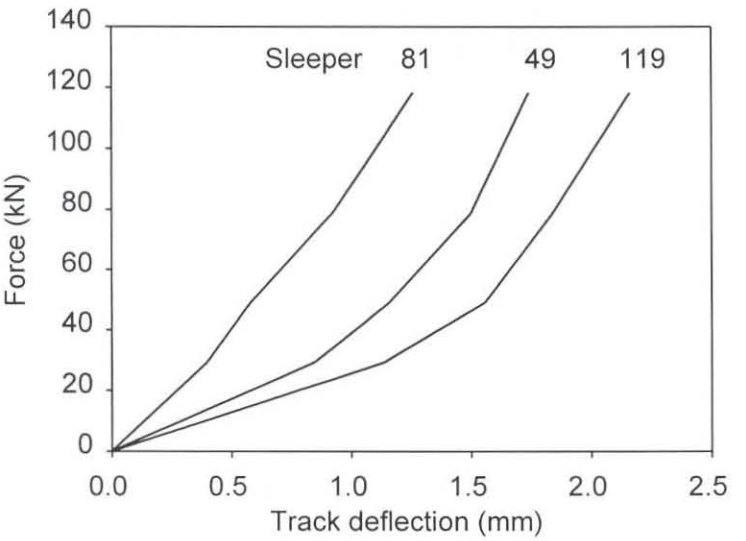


Figure B17: Static force-deflection curves.

### B.2.4 Track Instrumentation

To be able to analyse the dynamic behaviour of the track, wheel loads, sleeper reactions, and sleeper displacement measurements were taken at thirteen consecutive sleepers in the middle of the 150 sleeper test section. Using Multi-Depth-Deflection Meters (MDDs) (Maree, 1989), displacements in the various layers of the sub-structure were also measured at Sleeper 76. In Figure B18 a schematic layout of the instrumented test site shows the position of the strain gauges, the displacement transducers, the holes for the MDDs, and the displacement transducer frame with its anchor holes.

Due to the fact that both the sleeper reactions as well as the sleeper deflections were measured simultaneously while the test train, or for that matter any train running on that line, passed over the test site, it was possible to make an extensive study of the dynamic track stiffness at thirteen consecutive sleepers. Details with respect to the specific purpose of the instrumentation, together with a detailed description of the instrumentation and some sample measurements are given in the following sub-sections.

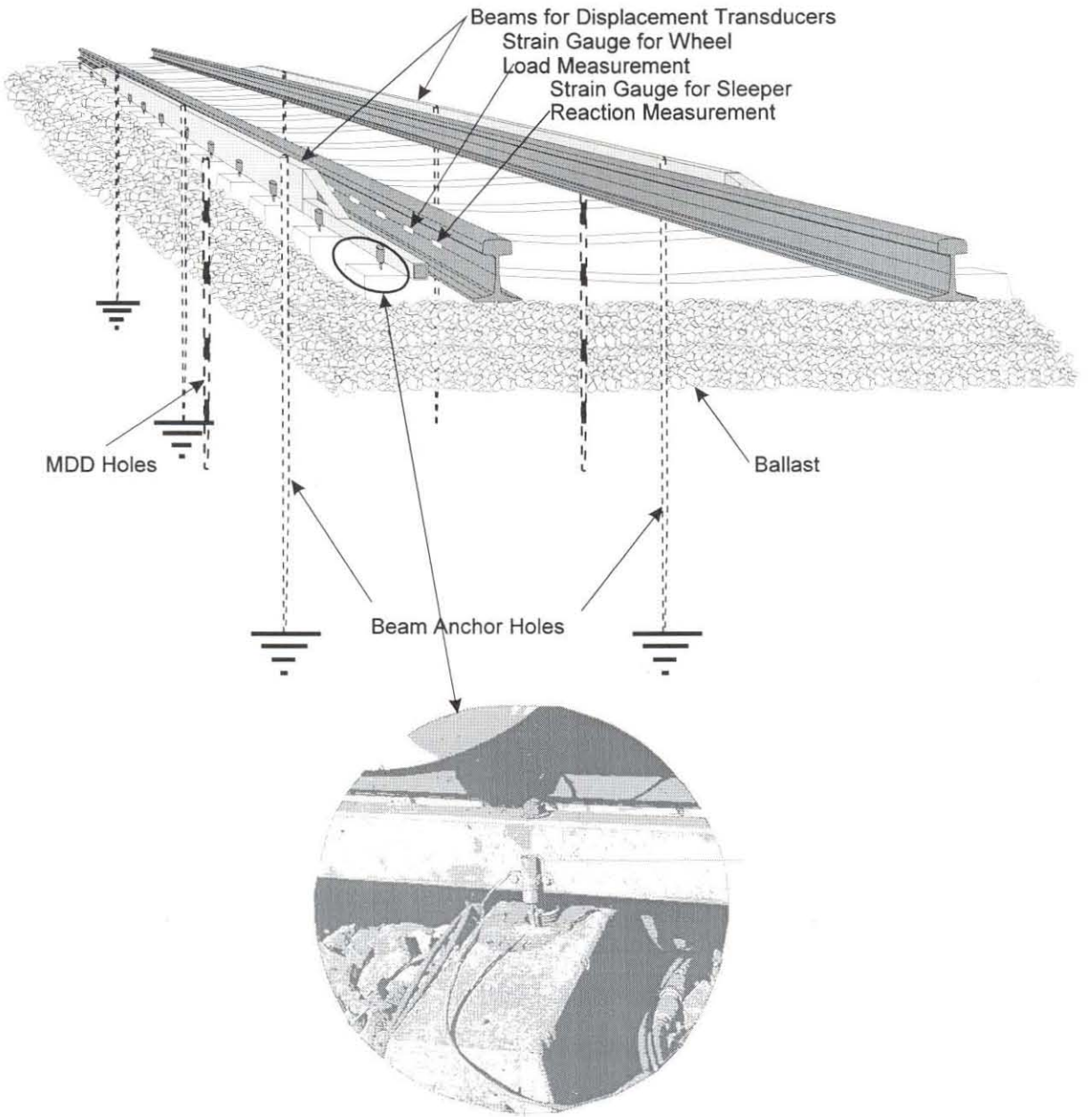


Figure B18: Layout of test track instrumentation.

*B.2.4.1 Purpose and Description*

Measurement of vertical sleeper displacement and sleeper reaction forces requires ingenuity. In 1994, Jeffs measured the rail seat load by inserting a water filled cell between the rail and the sleeper after having removed the existing rail pad. The

load cell was connected to a pressure transducer which then provided a signal proportional to the load transmitted through the cell. Jeffs measured the displacement of the sleeper using a laser system, with the reflector mounted on the sleeper. The laser system was placed 20m from the track and noise became a problem for an accuracy below 0.1mm.

The method used in this research makes use of a innovative combination of strain gauges on the rail and displacement transducers that measured the displacement between a reference frame and the sleepers. A detailed description of the instrumentation is given below.

*Strain gauges:* Vertical wheel loads and sleeper reaction forces were measured with shear strain gauges coupled into a full Wheatstone bridge circuit as shown in Figure B19. Reaction forces in the rail were determined by measuring the shear strain in the rail and converting it to the vertical reaction force (ORE Q D71 (Report 1), 1965). The strain gauge bridges were calibrated with a hydraulic ram and load cell to measure to an accuracy of 2%. To measure the dynamic vertical wheel load, these shear strain bridges were mounted on both rails between fourteen consecutive sleepers. To measure the dynamic sleeper reaction, additional shear strain bridges were mounted on both rails inline with the thirteen test sleepers. The measurements of the wheel load by the load measuring wheelset and by strain gauges on the rail were compared and found to deviate only slightly from one another. A comparison can be seen in Figure B20.

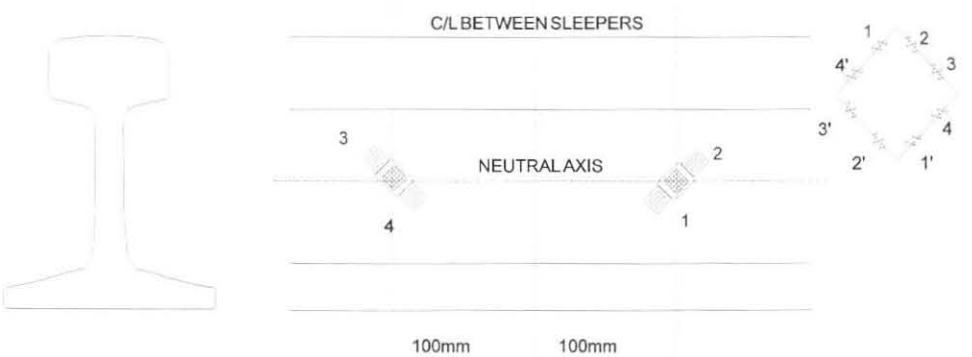


Figure B19: Position of shear strain gauges on the rail.

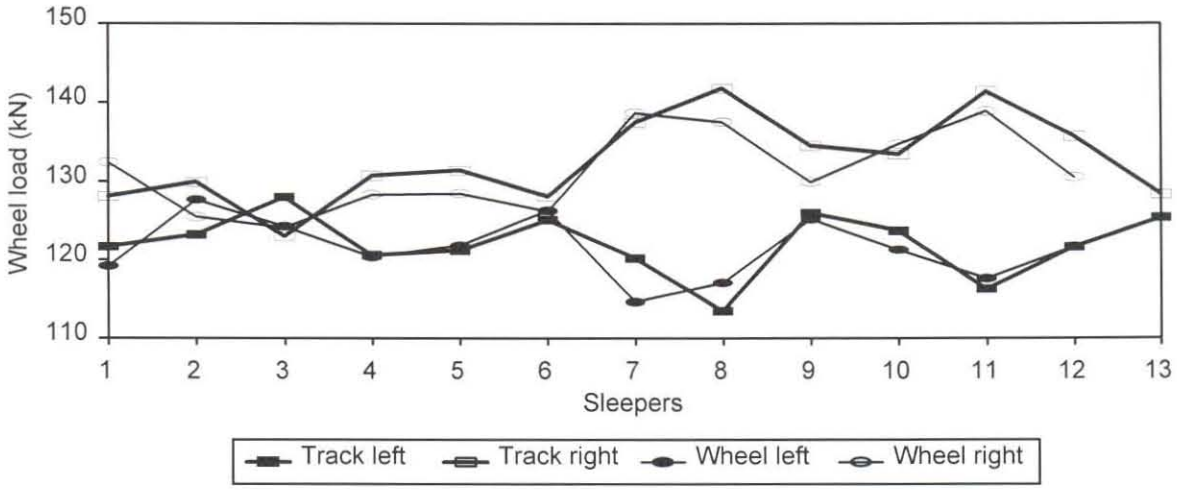


Figure B20: Comparison between wheel load as measured on track and by the load measuring wheelset.

*Displacement transducers:* Sleeper deflections were measured using displacement transducers mounted on a beam which was anchored at three positions 3.15 meters below the top of the sleepers as shown in Figure B18 and B21. The beam assembly was constructed, to be able to measure the absolute vertical displacement of thirteen sleepers on each side of the track as a train passes over the instrumented test site. Figure B21 shows the beam and displacement transducer mounting. 20mm inductive LVDTs were used to measure the relative displacement between the beam and the sleepers. The construction of the frame was such that the beam could be removed from its anchor rods before tamping the track or before measuring the stiffness of the track with the "BSSM" track loading vehicle.

*Multi-Depth-Deflectionmeters:* MDDs were installed on the left and right hand side of Sleeper 76 to electronically measure the vertical movement in the track sub-structure layers. Each of the two MDD holes as indicated in Figure B18 contained six measuring modules. These multi-stage sensors were used to measure resilient deflections and permanent deformation at various depths under loading from rolling stock relative to the anchor 3.15m below the rail. The displacement transducers used in the modules were the same as used on the beam and were calibrated to measure to a resolution of 0.01mm. Figure B22 shows the construction of a MDD

module and the instrumentation placed into the hole. MDDs for the use in track structures, were developed by Spoornet and the Council for Scientific and Industrial Research (CSIR) Division for Roads and Transport Technology (Maree, 1989).

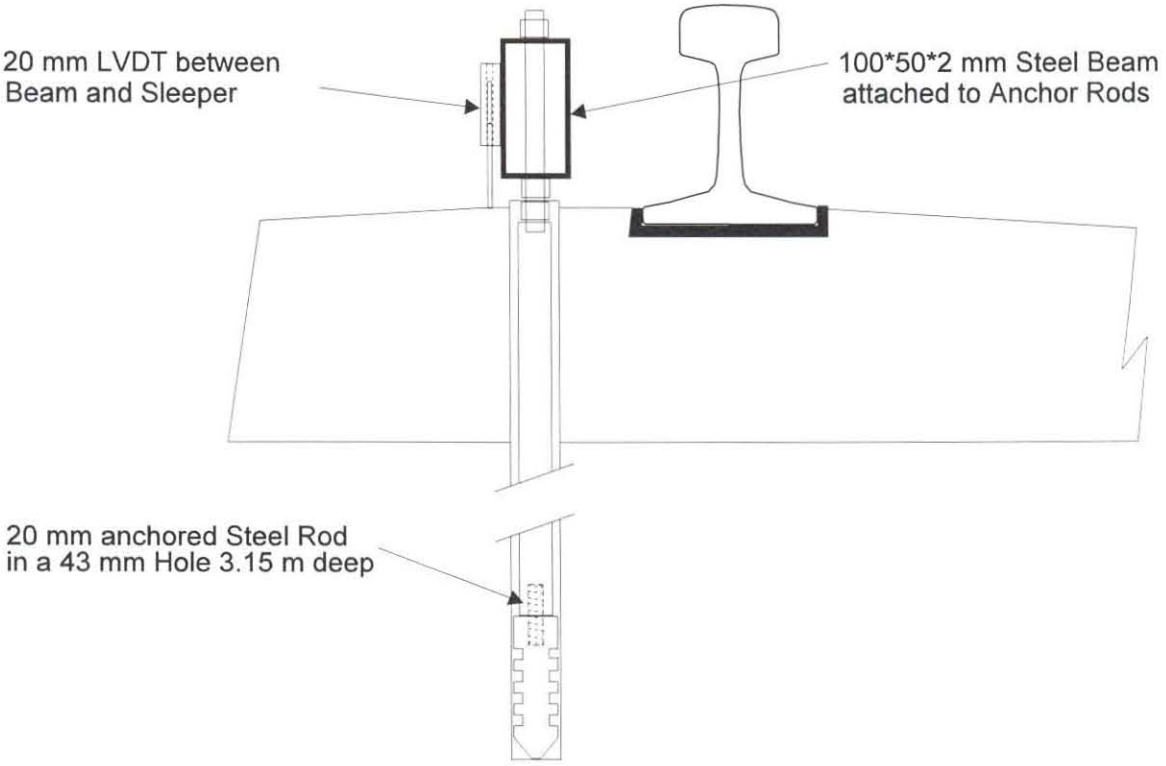


Figure B21: Beam and displacement transducer mounting.

The MDDs were placed into the sub-structure of the track to provide information required to determine the stiffness of the track and the properties of the different sub-structure layers using the program GEOTRACK (Chang *et al*, (1980)). Using the measured wheel loads and given track design parameters as input to GEOTRACK, layer deflections were calculated and compared to the layer deflections measured by the MDDs. Three to five iterations were usually enough to achieve a good convergence. Once a good comparison between the calculated and the measured results had been reached, the stiffness of the different structural layers and the modulus of elasticity was calculated. It was found that the ballast and first soil layer had a random variation in stiffness from test to test, but that the lower

layers provided very consistent results. Multiple wheel loads were used to determine the modulus of elasticity of the track sub-structure layers. A maximum of five layers can be handled with this program. The last layer is assumed to be of infinite depth.

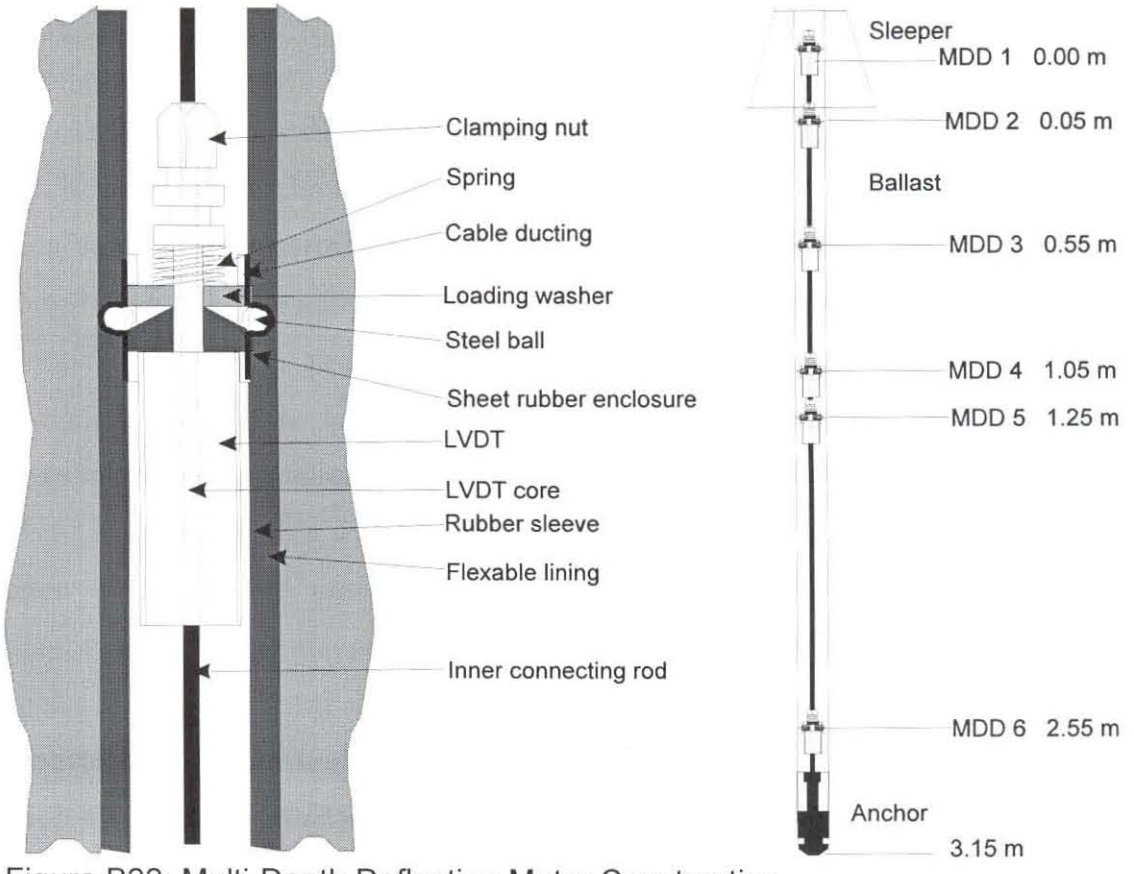


Figure B22: Multi-Depth Deflection Meter Construction.

*B.2.4.2 Sample Measurements and Interpretation*

In this section a selection of measurements are given. In the first example, the concept of determining the dynamic track stiffness from on-track measurements is shown. In the second part of this section the wheel loads, sleeper reactions and sleeper deflections are shown as the test locomotive passes over a selected sleeper in the test section. Furthermore, the deflections in the various sub-structure layers are also shown.

To obtain the dynamic behaviour of the track, there are basically three parameters to be observed. The parameters are the wheel load, the sleeper reaction, and the sleeper deflection due to a passing wheel. In Figure B23, measurements of these three parameters are shown. It can be seen that the wheel load was measured slightly before the sleeper reaction and sleeper displacement. This is due to the fact that the wheel load can only be measured between two sleepers, while sleeper reaction and sleeper displacement are measured while the wheel passes directly over the sleeper. As the rail between the sleepers only senses the wheel load as the wheel passes over the section measuring the shear strain, the wheel load shows a single and clearly defined spike. The sleeper reaction on the other hand has a more complex shape. The shape can be explained as follows. As the wheel approaches the sleeper where the shear strain is measured, the sleeper progressively starts carrying more of the load. As soon as the wheel is directly above the sleeper and thus in the section where the shear strain is measured, the measured load changes direction and shows a wheel load spike on top of the measured sleeper reaction. As soon as the wheel passes over the top of the sleeper the wheel load portion disappears and the sleeper reaction slowly decreases back to zero. Thus, to be able to determine the total sleeper reaction force, the wheel load measured just before a particular sleeper is mathematically shifted forward by half a sleeper spacing and then the sleeper reaction is subtracted from the wheel load to give the resultant effective sleeper reaction force against time. From Figure B23 it can be seen that the maximum sleeper reaction is about 45% of the actual wheel load. This is due to the fact that the adjacent sleepers carry part of the load.

In Figure B24 a dynamic force-deflection curve, or dynamic track stiffness curve is shown. This curve is obtained by plotting the resultant effective sleeper reaction force against the measured sleeper deflection. From Figure B24 it can be seen that the track stiffness is progressive and has a clearly defined hysteresis loop due to structural damping.

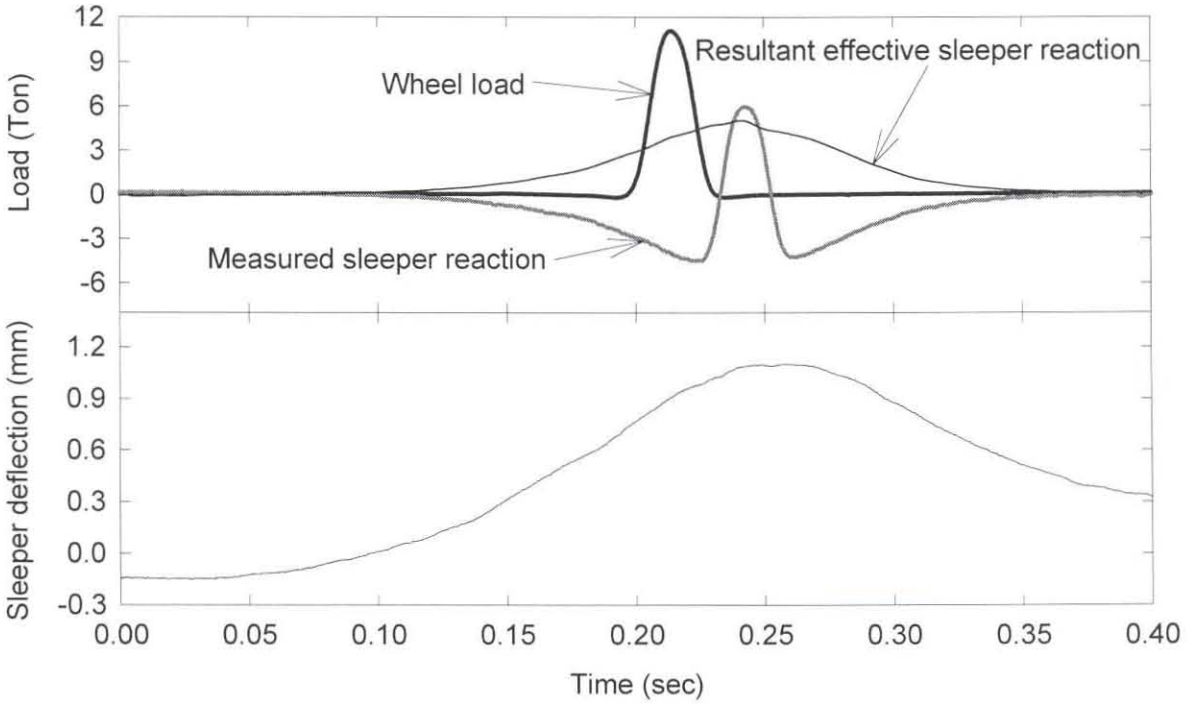


Figure B23: Measured dynamic track parameters.

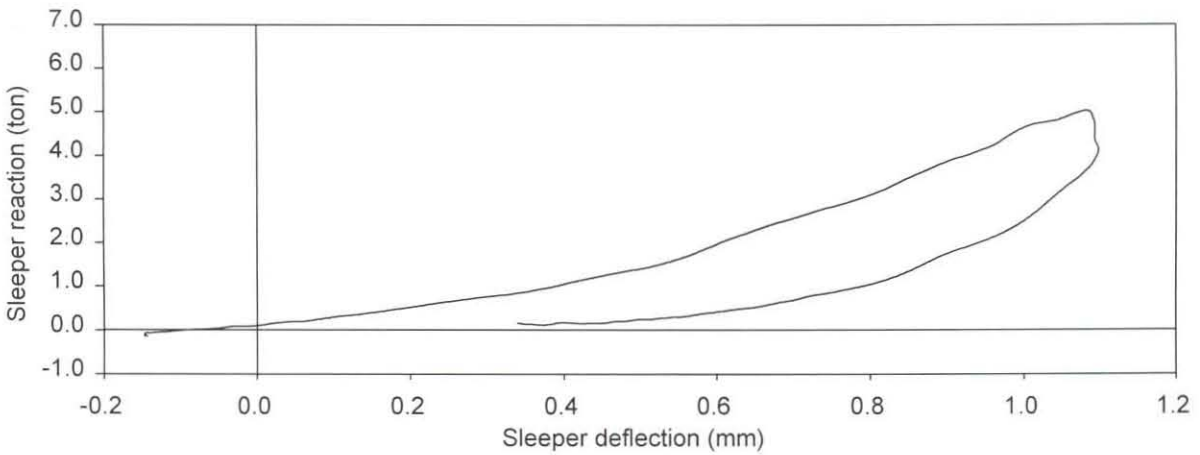


Figure B24: Dynamic track stiffness under one wheel.

To illustrate the behaviour of a selected sleeper in the test section as the test locomotive passes over it, the corresponding wheel loads, sleeper reactions and

sleeper deflections are shown in Figure B25. In Figure B26 the resultant dynamic track stiffness is shown. The deviation in the different dynamic track stiffness loops is due to a slight variation in the wheel loads of the locomotive. This can be due to the static load distribution of the locomotive as well as effects due to dynamic wheel loading.

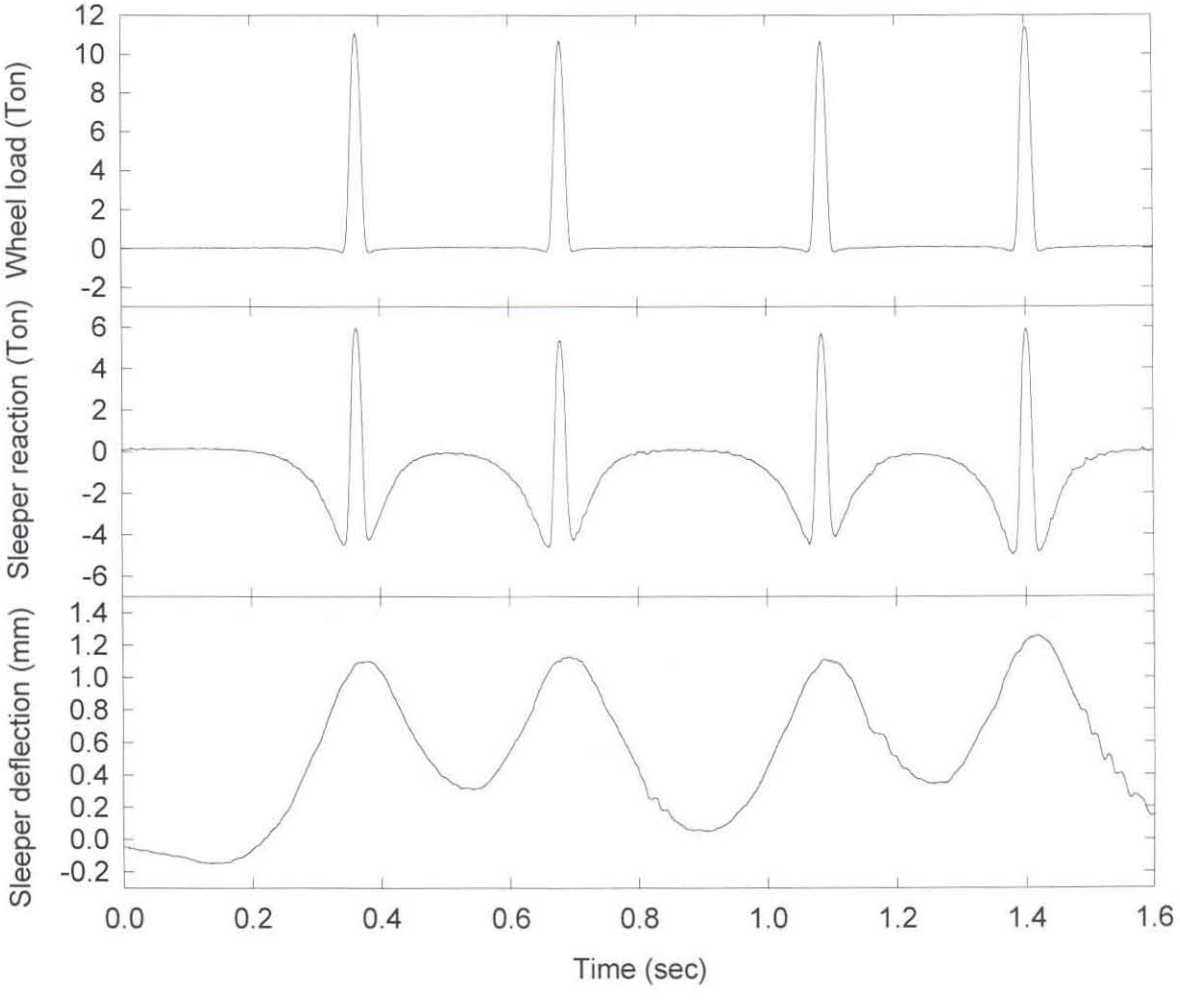


Figure B25: Track reaction due to a passing locomotive.

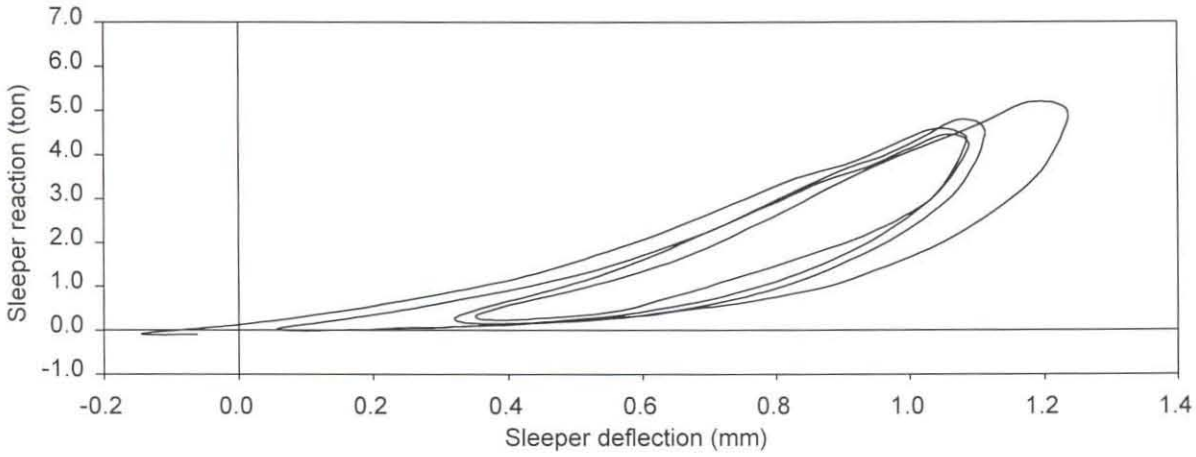


Figure B26: Dynamic track stiffness due to a passing locomotive.

In Figure B27 the cumulative deflections in the various sub-structure layers are shown as the locomotive passes over the MDDs at Sleeper 76. Considering the various layer thicknesses as shown in Figure B22, it is noted that the highest relative track deflection takes place in the ballast layer.

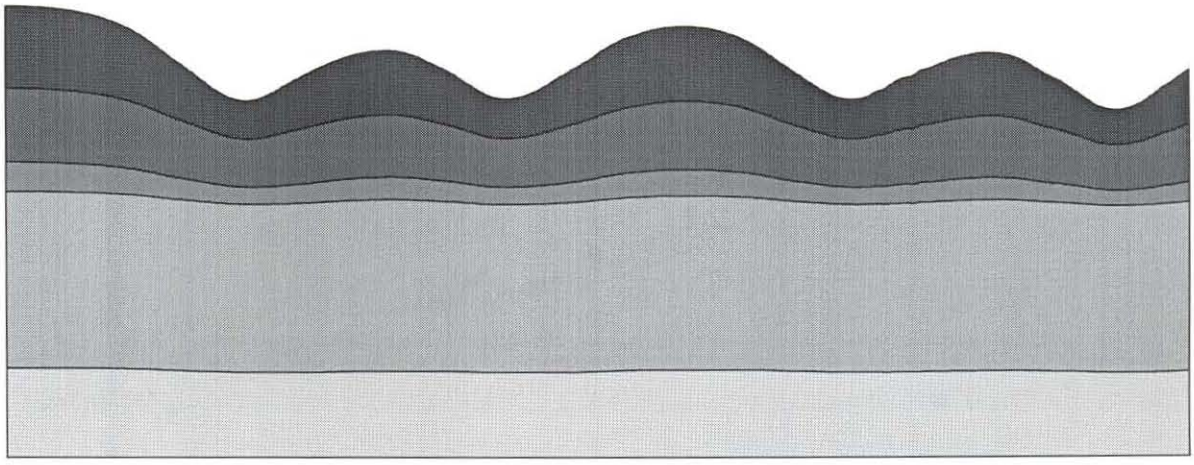

Figure B27: Deflection in sub-structure layers at Sleeper 76 as a function of time.

### B.2.5 Dynamic Track Stiffness

In Figure B28 examples of the dynamic track stiffness and the track damping properties as measured at four consecutive sleepers are given. Superimposed on the

dynamic load-deflection curve are the static load-deflection values as measured by the BSSM track loading vehicle. The static values are indicated by the little squares. From the plotted values it can be seen that there is good agreement between these two measuring techniques. Further research to establish whether the static values should be below, on or above the dynamic values is proposed. It should be noted that the sleeper reaction force and not the actual wheel load is plotted against sleeper deflection. The difference between the wheel load and the sleeper reaction force is due to a part of the wheel load being carried by adjacent sleepers.

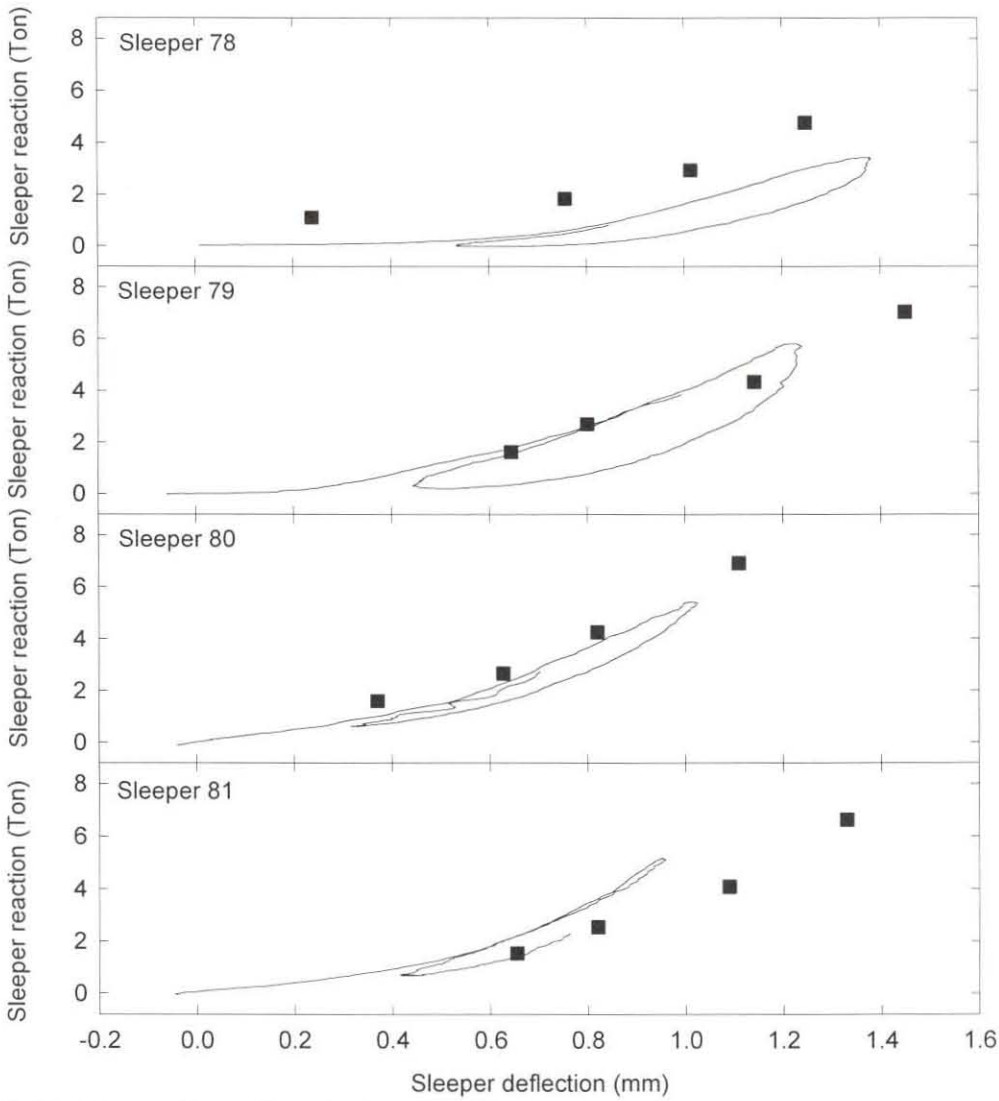


Figure B28: Dynamic and static track stiffness.